JOURNAL OF SPACECRAFT AND ROCKETS
Vol. 39, No. 4, July–August 2002

Initial Guess Generation for Rocket Ascent Trajectory Optimization Using Indirect Methods

Peter F. Gath* and Klaus H. Well†
University of Stuttgart, 70550 Stuttgart, Germany
and
Klaus Mehlem‡
European Space Research and Technology Center, 2200 AG Noordwijk ZH, The Netherlands

An approach for generating an initial guess for a direct optimization method in the field of rocket ascent trajectories is described. An indirect optimization approach is used to calculate a trajectory that neglects atmospheric effects, path constraints, and several other more complicated boundary constraints. Once this trajectory is generated, it is used as an initial guess for a direct optimization method, which includes all atmospheric effects, path, and boundary constraints. The indirect method also generates a switching function, which is used to analyze the nominal mission profile in order to identify possible improvements by adding coast arcs. Such an analysis is presented on an example mission of the European Ariane 5 launcher. For this mission the payload mass can be increased by 66% by adding one additional coast arc. Finally, the flexibility of the direct optimization method allows for various complicated boundary constraints such as dynamic pressure, heat flux, or empty stage splashdown constraints. In the example mission presented, enforcement of those constraints within the direct optimization is demonstrated.

Nomenclature

E	=	orbital energy, km^2/s^2
H	=	Hamiltonian
$\boldsymbol{i}_b$	=	unit vector along body axis
$\boldsymbol{i}_f$	=	unit vector perpendicular to the orbit plane, $(\boldsymbol{i}_R \times \boldsymbol{i}_V)/\lvert\boldsymbol{i}_R \times \boldsymbol{i}_V\rvert$
$\boldsymbol{i}_N$	=	unit vector pointing north
$\boldsymbol{i}_R$	=	unit vector along radius vector
$\boldsymbol{i}_V$	=	unit vector along inertial velocity vector
J	=	performance index
m	=	mass of vehicle, kg
$\boldsymbol{P}$	=	velocity costate vector/primer vector, s/m
p	=	magnitude of primer vector, s/m
$\boldsymbol{Q}$	=	position costate vector, 1/m
q	=	mass-flow rate, kg/s
$\boldsymbol{R}$	=	radius vector, m
r	=	norm of the radius vector, m
S	=	switching function
T	=	thrust, N
t	=	time, s
$\boldsymbol{V}$	=	inertial velocity vector, m/s
v	=	norm of the inertial velocity vector, m/s
α	=	angle of attack, rad
γ	=	flight-path angle, rad
η	=	throttle factor
λ_m	=	mass costate, 1/kg
μ	=	gravitational constant, m^3/s^2
ω	=	Schuler frequency, rad/s

Subscripts

a	=	apogee
b	=	body axis
d	=	desired value
f	=	final
p	=	perigee

Introduction

THE major advantage of trajectory optimization using direct methods with control discretization is the easy implementation of fairly complicated path and boundary constraints. Such constraints are mandatory for realistic mission scenarios. In addition, the adjoint differential equations are not required. Therefore, the equations of motion can easily be changed if necessary.

However, it is often very time consuming to supply an adequate initial guess for the controls in order to get convergence. A common approach is to use guidance laws to get a first estimate for the controls.[1] In this paper an indirect optimization method based on Refs. 2–7 is used to obtain a solution for an ascent without any path constraints. It turns out that it is sufficient to supply the solution for an ascent in vacuum to the direct optimization method in order to get convergence. For complex mission scenarios involving several coast arcs, the mission can be split into sub-missions for generating an initial guess with the indirect method. All sub-missions are merged together, and the final optimization is performed with the direct optimization code.

Neglecting the dissipative terms, such as atmospheric drag, makes the resulting two-point boundary-value problem easy to solve. Almost arbitrary values can be used as initial guesses for the unknown initial costates to achieve convergence. Similar observations are reported in Ref. 3. To ensure that the resulting trajectory is a feasible trajectory, a direct mulitple shooting method is used. In contrast to a direct collocation method, a direct multiple shooting method yields a nonlinear program with fewer optimization parameters and constraints.

As an example problem, a dual-payload mission with the European Ariane 5 launcher (Fig. 1) is presented in this paper. During the first 129 s, the main stage of this rocket is supported with two solid rocket boosters that include predefined, time-dependent thrust and mass-flow rate profiles. When using direct collocation methods in connection with such profiles, the discretization must be performed with great care by placing the collocation nodes exactly on the location of the thrust and the mass-flow rate profile data points.[8]

Presented as Paper 2000-4589 at the AIAA Guidance, Navigation, and Control Conference, Denver, CO, 14–17 August 2000; received 30 October 2000; revision received 6 March 2002; accepted for publication 13 March 2002.

*Ph.D. Student, Institute of Flight Mechanics and Control IFR, Pfaffenwaldring 7a; peter.gath@gmx.net. Student Member AIAA.
†Professor, Institute of Flight Mechanics and Control IFR, Pfaffenwaldring 7a; klaus.well@ifr.uni-stuttgart.de. Member AIAA.
‡Technical Officer; kmehlem@estec.esa.nl.

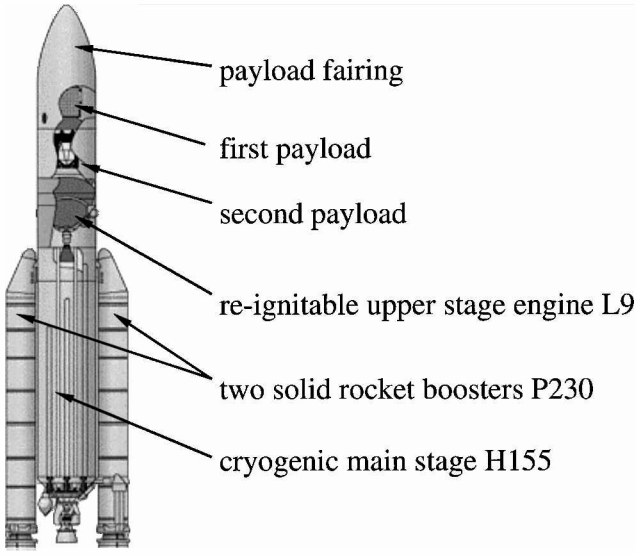

Fig. 1 Overview of the Ariane 5 launcher.

A wrong placement will lead to a significantly larger discretization error, and many additional collocation nodes are required to obtain a trajectory with a sufficient accuracy. In the framework of direct multiple shooting, the step-size control algorithm of the numerical integration method will automatically take care of this problem.

By analyzing the switching function obtained with the indirect method, improved mission profiles with an additional coast arc are identified. These improved mission scenarios are optimized with the direct optimization method and compared to the original setup.

Although it is sometimes possible to automatically remove unnecessary, additional burn arcs in the framework of a direct trajectory optimization method, it is usually hard to obtain an initial guess for such a setup without an a priori knowledge about the shape of the resulting trajectory. If the initial guess is too far from the optimal solution, the optimizer might remove an additional burn arc and find another, locally optimal solution with a reduced number of burns. By using the switching function analysis, such situations can easily be identified, and corrections can be applied until the structure of the switching functions shows an optimal sequence of burn and coast arcs.

The main objective of this paper is to demonstrate the possibility of using an indirect optimization method for a detailed optimality analysis in a simplified setup and the option to use such a trajectory as an initial guess for a direct optimization method. In the framework of the direct optimization method, all path and boundary constraints that are required for a realistic mission can easily be added to the scenario.

Indirect Optimization Method

This section briefly describes the indirect optimization method High-Speed Trajectory Optimization Software (HISTOS) as it is used for this study. A more detailed description can be found in Ref. 7. All variables have been normalized in the numerical implementation of the algorithm such that μ can be set to one as described in Ref. 5.

The dynamic system for an ascent in vacuum is

$$\begin{bmatrix} \dot{\boldsymbol{V}} \\ \dot{\boldsymbol{R}} \\ \dot{m} \end{bmatrix} = \begin{bmatrix} -\omega^2 \boldsymbol{R} + (\eta T/m)\boldsymbol{i}_b \\ \boldsymbol{V} \\ -\eta q \end{bmatrix} \tag{1}$$

The control is the direction of thrust, represented by the unit vector $\boldsymbol{i}_b$. η is a throttle factor, which becomes zero during coast arcs and one during burn arcs. As it was mentioned in the Introduction, thrust T and mass-flow rate q can be user-supplied functions of time. Such profiles are not considered as being free for optimization, but as predefined thrust and mass-flow rate programs as they usually occur in the framework of solid rocket boosters. To simplify the further discussion, a constant thrust T and mass-flow rate q are assumed.

To integrate the trajectory almost analytically,[4–7] a linear gravity field is used. ω is the Schuler frequency, defined as $\omega = \sqrt{(\mu/r_{\text{ref}}^3)}$, where r_{ref} is a reference radius. In this application the Earth radius is used as a reference.

With the Lagrange cost term set to zero, the Hamiltonian of the optimal control problem is defined as

$$H = \boldsymbol{P}^T\left[-\omega^2 \boldsymbol{R} + (\eta T/m)\boldsymbol{i}_b\right] + \boldsymbol{Q}^T \boldsymbol{V} - \lambda_m \eta q \tag{2}$$

where $\boldsymbol{P}$, $\boldsymbol{Q}$, and λ_m represent the costates. Based on Eq. (2), the adjoint differential equations can be derived as

$$\begin{bmatrix} \dot{\boldsymbol{P}} \\ \dot{\boldsymbol{Q}} \\ \dot{\lambda}_m \end{bmatrix} = \begin{bmatrix} -\boldsymbol{Q} \\ \omega^2 \boldsymbol{P} \\ (\eta T/m^2)\left(\boldsymbol{i}_b^T \boldsymbol{P}\right) \end{bmatrix} \tag{3}$$

It turns out that λ_m is not required during the solution process and can therefore be disregarded.

The optimal control for an ascent in vacuum is $\boldsymbol{i}_b = \boldsymbol{P}/p$, which is a well-known result in the classical literature on spacecraft trajectory optimization.[2,3] It is assumed that all initial states are known. The initial costates are computed such that the final states and costates satisfy the final boundary constraints and the transversality conditions. The final orbit is defined by its apogee radius, perigee radius, and inclination. The remaining orbital parameters are considered as being optimizable.

To be able to propagate the trajectory in an almost analytic form[4] and to keep the formulation of the required Jacobian matrix (the sensitivity of the final states and costates with respect to the initial states and costates) simple, the problem is reformulated as a fixed final time problem. In the new problem formulation only the inclination and the perigee radius are enforced when solving the two-point boundary-value problem. The final orbital energy

$$J = E = v_f^2/2 - \mu/r_f \tag{4}$$

is maximized.

The detailed equations for the final boundary constraints and transversality conditions can be found in Refs. 4–7. For a circular target orbit with an inclination of i_d and a radius of $r_{p,d}$, the following set of terminal constraints and transversality conditions can be used:

$$\psi = \begin{bmatrix} \boldsymbol{i}_f^T \boldsymbol{i}_N - \cos i_d \\ r - r_{p,d} \\ \boldsymbol{R}^T \boldsymbol{V} \\ \dfrac{\boldsymbol{i}_f^T(\boldsymbol{i}_N \times \boldsymbol{V})}{\boldsymbol{i}_f^T(\boldsymbol{i}_N \times \boldsymbol{R})} \boldsymbol{P}^T \boldsymbol{i}_f + \boldsymbol{Q}^T \boldsymbol{i}_f \\ \boldsymbol{P}^T \boldsymbol{i}_R - \dfrac{r}{v} \boldsymbol{Q}^T \boldsymbol{i}_V \\ \boldsymbol{P}^T \boldsymbol{i}_V - v \end{bmatrix} \tag{5}$$

A simple Newton method with step-size control is used to solve the two-point boundary-value problem. Starting with arbitrary guesses for the initial costates, convergence is usually achieved within 20 iterations. Such an optimization yields a trajectory with a maximum final orbital energy. A detailed analysis on the convergence radius is not performed. However, the convergence radius seems to be very large because no problems were encountered in choosing an initial guess for the costates. Similar observations are also made in Ref. 3. Note that $\boldsymbol{P}$ must not be set to the null vector because the optimal control vector is computed as the unit vector along $\boldsymbol{P}$.

Depending on the mission, either the burn time is minimized, or the payload mass is maximized in an outer loop. In other words, once the two-point boundary-value problem is solved, the final orbital

energy is compared to the required orbital energy calculated from the desired apogee and perigee radius as

$$E_d = -\mu/(r_{p,d} + r_{a,d}) \tag{6}$$

Then, either burn time or initial mass are modified, and the two-point boundary value problem is solved again until the deviation between final orbital energy and desired orbital energy becomes less than a user-specified value. The required changes in the burn time or in the initial mass are computed according to the following two sections.

Approach for Minimizing Burn Time

According to Ref. 9, the variation in the performance index due to a variation in final time can be expressed as

$$\delta J = H_f \delta t_f \tag{7}$$

Because neither any terminal constraint nor the performance index J depends on final mass, the final value of its associated costate λ_m has to be zero at final time. Therefore, δt_f can be calculated as

$$\delta t_f = \frac{\delta J}{H_f} = \frac{-\mu/(r_p + r_a) - \left(v_f^2/2 - \mu/r_f\right)}{-\boldsymbol{P}^T(\mu \boldsymbol{R}/r^3) + (T/m)\boldsymbol{P}^T \boldsymbol{i}_b + \boldsymbol{Q}^T \boldsymbol{V}} = \frac{E_d - E}{H_f} \tag{8}$$

The necessary correction predicted by Eq. (8) is limited to a user-definable value. For the Ariane 5 launcher, 20–30 s has proven to be a reliable value. The two-point boundary-value problem is then solved using the new burn time until the required accuracy in the final orbital energy is achieved. Because very good guesses for the initial costates are already available, only one to three Newton iterations are required for such an update.

Approach for Maximizing Payload

If burn time is to be kept constant and the payload mass has to be maximized, the algorithm calculates the necessary change in the final mass. First, Eq. (4) is differentiated with respect to time, which yields

$$\dot{E} = v\dot{v} + \mu v \sin\gamma / r^2 \tag{9}$$

If thrust is assumed to be aligned with the velocity vector, the conservation of momentum can be written as

$$m\dot{v} = T - \mu m \sin\gamma / r^2 \tag{10}$$

In case thrust is not aligned with the velocity vector, T would have to be replaced by $T\cos\alpha$. However, Eq. (10) is a good approximation even for large angles of attack. Substituting $\dot{v}$ in Eq. (9) with Eq. (10) yields

$$\dot{E} = Tv/m \tag{11}$$

which can also be written as

$$\frac{\mathrm{d}E}{\mathrm{d}m}\frac{\mathrm{d}m}{\mathrm{d}t} = \frac{Tv}{m} \tag{12}$$

Thrust and mass-flow rate are assumed to be constant, which usually is the case for an upper stage engine. If velocity is also assumed to be constant, Eq. (12) can be integrated. The result is the necessary change in final mass:

$$\Delta m_f = m_f \left\{ \exp\left[\frac{-(E_d - E)q}{Tv}\right] - 1 \right\} \tag{13}$$

Because thrust T and mass-flow rate q are state independent and the burn time is fixed, $m_f - m_0$ is constant for all possible trajectories. Therefore, Δm_f in Eq. (13) is equivalent to the required change in the initial mass Δm_0.

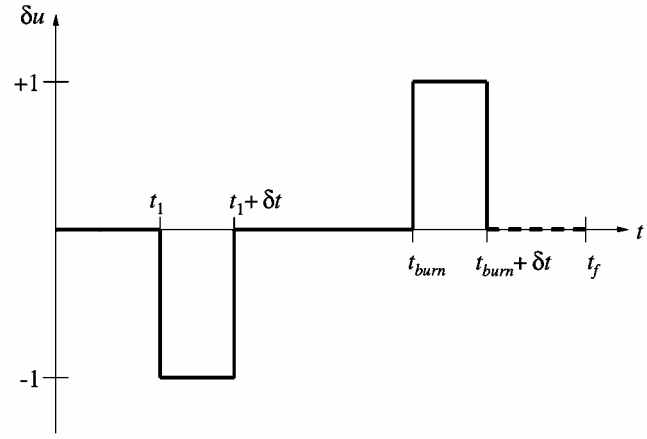

Fig. 2 Changes in the control u when adding an additional coast arc.

Switching Function

The control η appears linearly in the Hamiltonian [Eq. (2)]. Therefore, it is optimal when it is either on its upper bound (burn arc) or lower bound (coast arc). The possibility of a singular arc, where η is between its bounds, is excluded by assumption. The switching function shows whether a burn arc is optimal or if additional coast arcs should be added. By writing the thrust-dependent part of the Hamiltonian as

$$H = \eta S(T) + \text{other terms} \tag{14}$$

where $0 \le \eta \le 1$ is the throttle, a switching function can be calculated as

$$\frac{\partial H}{\partial \eta} = S = \frac{\boldsymbol{P}^T \boldsymbol{i}_b}{m} T - \lambda_m q \tag{15}$$

Without a loss in generality, one can assume that a trajectory ends on a coast arc and final time is fixed. According to Ref. 9 and using Eq. (15), the variation in the performance index caused by variations in the scalar control η can be written as

$$\mathrm{d}J = \int_{t_0}^{t_f} (S\delta u)\,\mathrm{d}t \tag{16}$$

If a small coast arc of length δt_1 is inserted at t_1, where $t_0 < t_1 < t_{\text{burn}}$, the necessary δu is -1 at this point. Because burn time is kept constant, the end of the second burn will be at $t_{\text{burn}} + \delta t_{\text{burn}}$, where $\delta t_{\text{burn}} = \delta t_1$ and δu at this point is $+1$ (Fig. 2). Now, Eq. (16) can be written as

$$\mathrm{d}J = [S(t_{\text{burn}}) - S(t_1)]\delta t_1 \tag{17}$$

If the current solution is already optimal, $\mathrm{d}J$ has to be less or equal to zero for an arbitrary δt_1. On the other hand, if a new coast arc is inserted δt_1 is greater than zero. Therefore, if the performance index J is to be maximized $\mathrm{d}J$ has to be less or equal to zero for a positive δt_1 if the current solution is already optimal.

In other words, $S(t_1)$ has to be greater or equal to $S(t_{\text{burn}})$ at all times $t_1 < t_{\text{burn}}$:

$$S(t_1) \ge S(t_{\text{burn}}) \tag{18}$$

If Eq. (18) is not satisfied during a burn arc, an additional coast arc could increase the performance index. This feature will later be exploited to improve the payload performance in the example mission scenario.

Direct Optimization Method

The direct optimization method transforms the infinite dimensional optimal control problem into a finite dimensional problem by discretizing the control with piecewise linear functions. The optimization algorithm that is used in this study is the Collocation and Multiple Shooting Trajectory Optimization Software (CAMTOS)

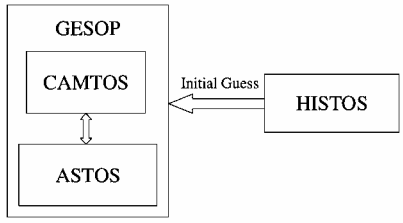

Fig. 3 Program structure.

and is described in more detail in Ref. 8. CAMTOS allows for a combination of direct collocation and multiple shooting within a multiphase trajectory optimization problem. In the framework of this study, all phases are discretized as multiple-shooting phases. Path constraints are enforced at certain path constraint evaluation points that have to be specified by the user.

The dynamics are implemented in the AeroSpace Trajectory Optimization Software (ASTOS)[10–13] and include all aerodynamics and a more detailed gravity model with J_2 terms. ASTOS is a completely data-driven implementation of launch and reentry vehicle dynamics, including a wide choice of path constraints, boundary constraints, and cost functions.

Both CAMTOS and ASTOS are embedded in the Graphical Environment for Simulation and Optimization (GESOP).[14,15] Within this environment it is possible to perform the whole grid specification, optimization, and simulation interactively by using a graphical user interface (Fig. 3).

State and control grid points, which are required for the direct optimization, can be initialized by using either guidance laws to generate an initial trajectory by running a simulation,[1] or by reading an existing trajectory data file. For this study the latter option is used to read the trajectory and control data that are generated by the indirect method HISTOS. It is essential for the convergence behavior of CAMTOS that the multiple shooting points are also initialized using the state values from the initial guess trajectory. Once all parameters are initialized, the optimization can be started.

Nominal Test Mission Scenario

The nominal test mission scenario presented in this paper is a dual-payload mission for the European Ariane 5 launcher (see Fig. 1) using a reignitable upper stage L9. The Ariane 5 vehicle consists of two solid rocket boosters P230 that burn in parallel to the cryogenic main stage H155 during the first 129 s. After the two P230s are jettisoned, only the H155 stage burns. After burnout of the main stage at 567 s into the flight, the L9 engine is ignited (see also Fig. 4).

The objective of this mission is to deliver two payloads in two different orbits where the mass of the second payload is maximized. The first payload with a fixed mass of 3000 kg has to be delivered in a 600-km circular orbit with 7-deg inclination. The second payload is then injected into a highly elliptic orbit with an apogee of 35,800 km and an argument of perigee of 270 deg. The launch site is Kourou. Because an argument of perigee of 270 deg has to be met for the second payload's target orbit, a coast arc is required after the first payload is delivered into its orbit.

There are certain additional path and boundary constraints that need to be satisfied. First of all, the dynamic pressure must not exceed 30 kPa during the whole mission. This path constraint becomes active once during the first 129 s. Second, the jettisoning of the payload fairing is triggered by a heat-flux value of 1135 W/m^2. Finally, the enforcement of a splashdown constraint is demonstrated. The H155 main tank is forced to splash down behind a line parallel to the coastline of the east coast of Africa.

The altitude profile of the whole mission is shown in Fig. 4. The solution shown is the final result obtained with the ASTOS model. There is a slight drop in the altitude profile during the coast arc, which is caused by the oblateness of the Earth.

Generating the Initial Guess

The implementation of the indirect optimization method does not allow any intermediate point constraints. Therefore, the mission is split into two sub-missions. The first mission is equivalent to the first burn arc, which delivers the first payload into its orbit. After engine cut off, a coast arc of fixed duration is added. The duration of this coast arc is only an initial guess and will later be optimized by CAMTOS such that the argument of perigee constraint is satisfied.

The second mission starts at the end of the coast arc and delivers the second payload into its target orbit. For the indirect optimization method the argument of perigee constraint is not enforced. However, it will be satisfied during the direct optimization.

Because the data from the indirect optimization are only used as an initial guess, they might have jumps in the states, for example, mass. For both sub-missions the payload mass is maximized. However, the lack of atmosphere during the first part of the mission increases payload so much that the second part would become infeasible. Therefore, the initial guess for payload mass is reduced before the second sub-mission is optimized. After both sub-missions are optimized with HISTOS, the trajectory data files are merged together, and the resulting trajectory can be used as an initial guess for the direct optimization method. CAMTOS converges within 46 iterations.

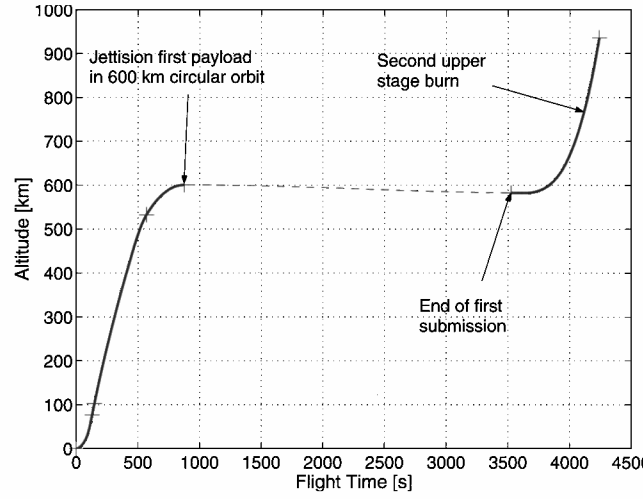

Fig. 4 Optimized altitude profile of the nominal mission scenario.

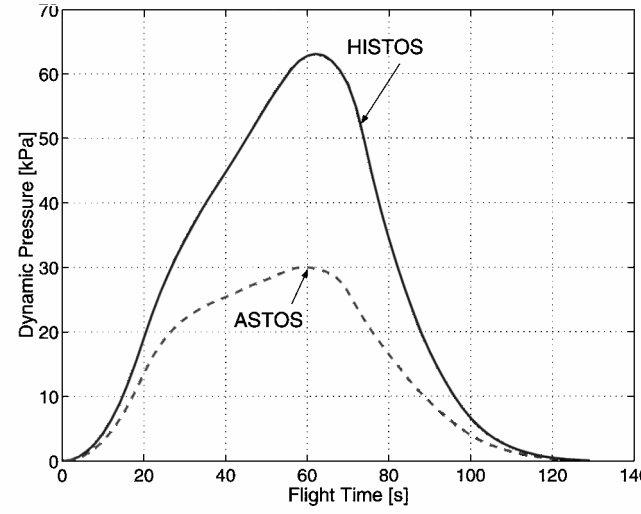

Fig. 5 Dynamic pressure in the first ascent phase.

Optimization Results for Nominal Mission

As just mentioned, Fig. 4 shows the final altitude profile. Several constraints have been enforced with the direct optimization. Figure 5 shows that the dynamic pressure profile along the trajectory generated by HISTOS clearly violates the dynamic pressure constraint, whereas it is satisfied in the ASTOS solution. The same applies to the splashdown constraint shown in Fig. 6. The unconstrained impact (HISTOS solution) occurs in a forbidden region.

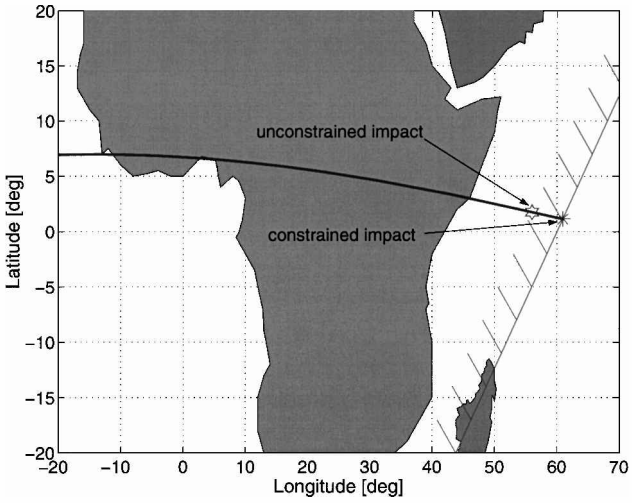

Fig. 6 Splashdown of the H155 stage.

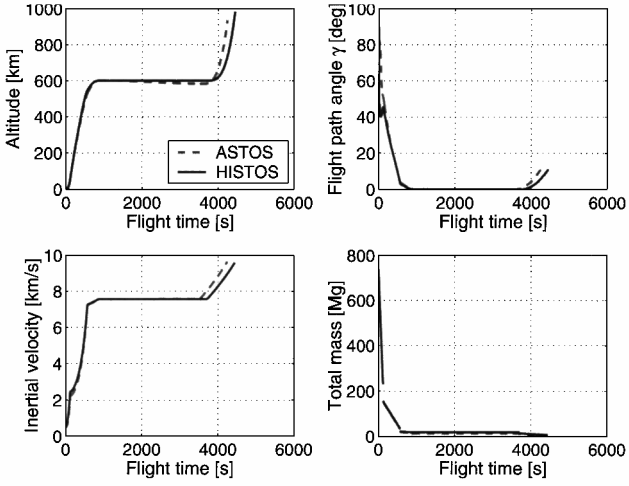

Fig. 7 Comparison of the state time histories.

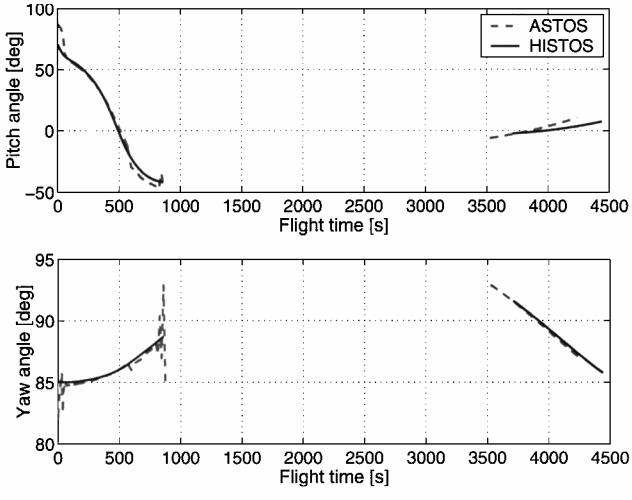

Fig. 8 Comparison of the control time histories calculated by ASTOS and HISTOS.

Figure 7 shows a comparison between the state profiles of the initial guess and the final solution. Note that the major differences occur only as a result of a different timing of the second burn. This burn has to be adjusted in order to meet the argument of perigee constraint of the second payload's orbit. The mass of the second payload is calculated as 1938 kg.

The controls yaw and pitch are shown in Fig. 8. Of course, there is a difference as a result of the missing atmosphere in the HISTOS solution. In addition, the timing of the second burn is different and, because the splashdown and the dynamic pressure constraint are only enforced in the ASTOS solution, additional deviations can be observed.

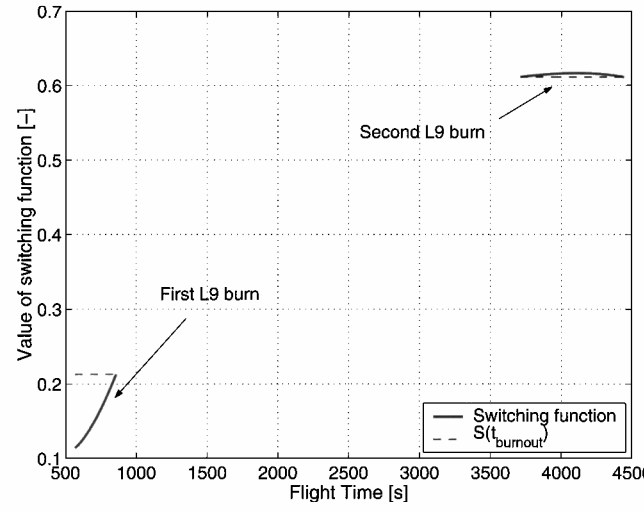

Fig. 9 Switching function profile during the nominal mission.

Analysis of the Switching Function

Figure 9 shows the profile of the switching function during the two upper-stage burns. Because two sub-missions have been optimized with the indirect optimization method, there exist two different values for the switching function at burnout. Note that the values of the switching function indicate an optimal performance during the second burn arc (3700–4500 s). However, the values of the switching function are clearly below its burnout value for the end of the first burn arc (500–900 s). Not shown in this plot is the switching function during the first 500 s. Its value is an order of magnitude larger than the burnout value of the switching function. The fact that S is below its burnout value at the beginning of the first upper-stage burn suggests that an additional coast arc right after the burnout of the H155 stage could improve the performance index.

Modified Test Mission Scenario

According to the results found for the nominal mission, the mission profile is changed by adding an additional coast arc after the burnout of the H155 stage. Again, the mission was split into two sub-missions in order to generate an initial guess using HISTOS. A coast arc of fixed duration was inserted after the H155 burnout. The altitude profile of the final ASTOS result for this modified test case is shown in Fig. 10. The altitude drops and rises again during the second coast arc because of the oblateness of the Earth.

Creating a New Initial Guess

To generate an initial guess, the mission profile is split into two sub-missions again. Now, the first sub-mission includes a coast arc of fixed duration right after H155 burn out. The duration of this coast arc is estimated based on the assumption that the apogee altitude is 600 km and perigee altitude is 100 km. The period of such an orbit can then be calculated as

$$P = 2\pi\sqrt{[(r_a + r_p)/2]^3/\mu} \tag{19}$$

which results in 5554 s. Half of this orbital period was used as an initial guess for the fixed-duration coast arc. However, the switching function for the second burn started slightly above its final value. Therefore, the duration of this coast arc was reduced to 2745 s until the optimality condition was almost met. This procedure could easily be done automatically, but because the final optimization is done by using the direct optimization method an accurate result for the switching times is not required at this point.

After the first sub-mission the vehicle is in a 600-km circular orbit. The duration of the second coast arc has been estimated to

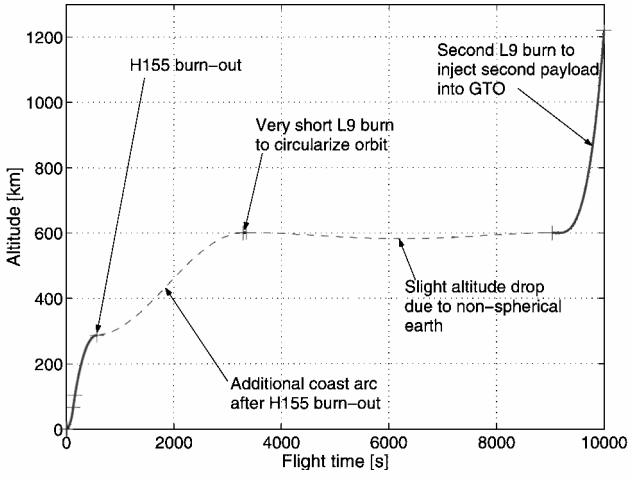

Fig. 10 Optimized altitude profile in the modified mission scenario.

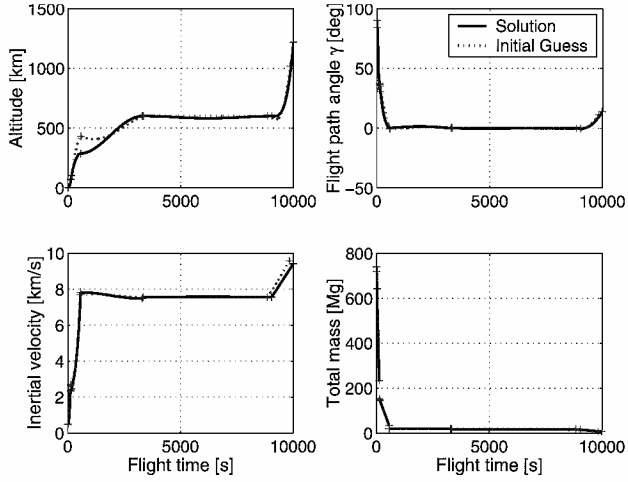

Fig. 11 State profiles in the modified mission scenario.

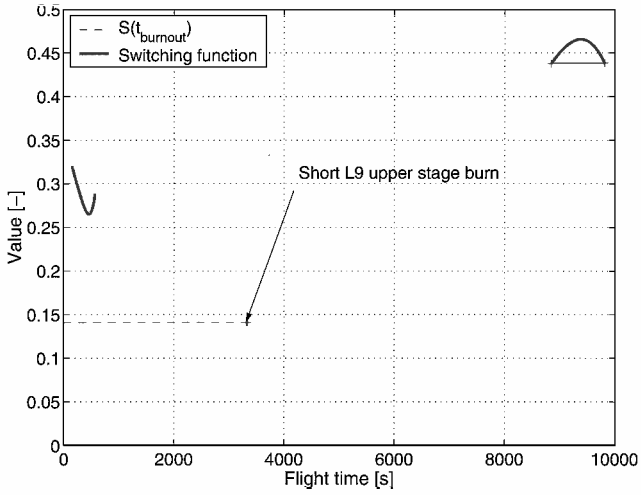

Fig. 12 Switching function in the modified mission scenario.

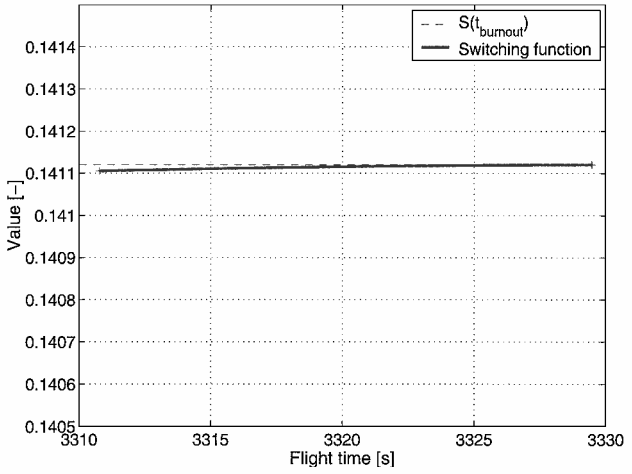

Fig. 13 Switching function during the second upper-stage burn.

5500 s, which is slightly less than a full revolution around the Earth. This long coast arc is required in order to meet the argument of perigee constraint for the second orbit later. The value can easily be estimated based on the position of the vehicle at the end of the second burn, and the position of the vehicle at the beginning of the burn arc required for the second payload that was calculated for the nominal mission scenario.

The second sub-mission is a single burn arc to achieve the correct apogee for the second payload. The argument of perigee constraint for the final target orbit is not enforced for the initial guess but will be enforced within the direct optimization.

Intermediate Optimization Results

Because the perigee of the first transfer orbit is too high for a reentry of the main tank, the splashdown constraint was not enforced in this modified mission. However, all other constraints, such as heat flux and dynamic pressure, were enforced. Figure 11 shows a comparison between the state profiles of the initial guess created with HISTOS and the final optimization results obtained with ASTOS. Now, there is a larger difference in the profiles, especially for the altitude. However, CAMTOS converges very rapidly within 47 iterations. The payload mass was calculated as 3840 kg, which is almost twice as much compared to the nominal mission.

Figure 12 shows the profile of the switching function computed with HISTOS. Note that there are two burnout values again because two sub-missions have been optimized. It can clearly be seen that the very short second burn is lying on the burnout value of the switching function. A magnification of this region is shown in Fig. 13. The value of the switching function is almost constant. A small deviation of about 10^{-4} can be observed when using greater magnification.

Reactivating the Splashdown Constraint

To avoid unnecessary space debris, a final modification to the mission profile is performed. The splashdown constraint has to be enforced again, such that the H155 main tank will return to Earth after burnout. However, the calculation of the splashdown constraint will fail because the perigee altitude after the H155 burnout is too high in the modified mission profile. If the H155 stage is supposed to deorbit, the perigee at burnout time must be below the Earth's surface. Therefore, an additional upper stage burn is added right after H155 burnout.

The splashdown constraint is now reactivated in two steps. First, the perigee altitude after H155 burnout is constrained to be −200 km or less. The additional upper-stage burn is required to aim the vehicle to its 600-km target orbit (Fig. 14).

This intermediate setup is initialized using the trajectory data from the preceding mission. Of course, these trajectory data do not include any upper-stage burn right after H155 burnout, but ASTOS just requires position, velocity, and attitude controls for the initialization.

After 10 iterations in CAMTOS, the optimization process is stopped, and the trajectory is simulated using a multiple shooting integration. Because convergence is not achieved yet, the result will show some jumps at the multiple shooting points. However, the perigee altitude after the H155 burnout is now below the Earth's surface, and the splashdown constraint can now be enforced. CAMTOS is reinitialized using the intermediate trajectory, and convergence can now be achieved. The constraint on perigee altitude after the H155 burnout is not enforced anymore. However, it was necessary to require a minimum perigee altitude of 200 km for the first coast arc in order to avoid a reentry of the upper stage. To get comparable results, a splashdown of the H155 stage was

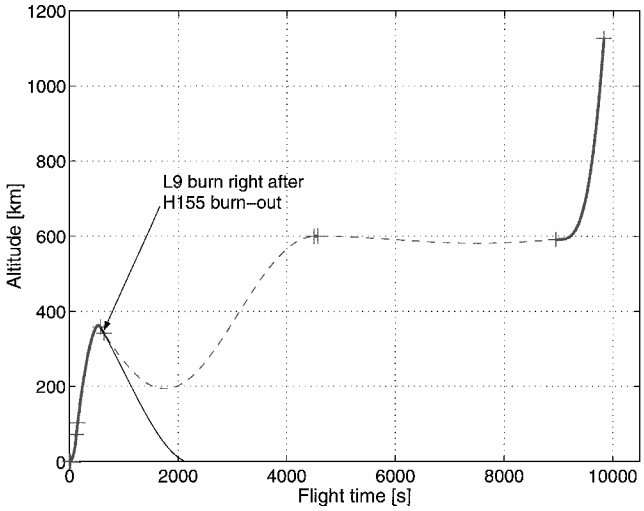

Fig. 14 Altitude profile of the modified mission scenario with splashdown constraint.

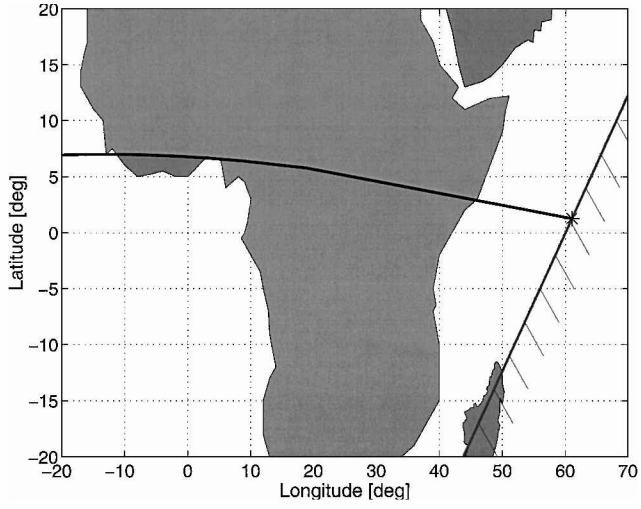

Fig. 15 Splashdown of the H155 stage in the final mission scenario.

requested in the same region as for the original mission profile (Fig. 15).

The payload mass is now reduced to 3222 kg. This value is 618 kg less payload than in the preceding result without a splashdown constraint, but it is still 1284 kg more than for the original mission profile.

Conclusions

The indirect optimization method HISTOS, which has been used to generate an initial guess, shows a very robust behavior when arbitrary initial guesses for the initial costates are used. It is a little bit more sensitive as far as an estimation on burn time or payload mass is concerned, but in general an adequate guess for these values can easily be provided.

The direct optimization method CAMTOS converges very rapidly using the initial guesses supplied by HISTOS. A near-optimal solution is calculated within a few iterations. Most time is spent to achieve a high accuracy for the final result, which is mainly caused by inaccurate gradient calculations caused by the interpolation of tabulated data for thrust, mass-flow rates, aerodynamics, and atmospheric data.

The ASTOS model has shown great flexibility when mission profiles were modified. Especially the setup, optimization, and analysis of the final mission profile have been generated in only about half a day, without the necessity of generating complicated initial guesses.

Using the approach discussed in this paper, the payload performance of the Ariane 5 vehicle for a given mission scenario has been improved significantly. The switching function, which was calculated as a byproduct of the indirect optimization method, clearly showed that the original setup was not optimal. Based on this conclusion, an improved mission profile is created, which finally yields a solution that satisfies all constraints and leads to an almost 66% increase in the payload mass compared to the nominal mission scenario.

Future research will focus on a tighter integration of the indirect optimization method into the ASTOS library. Such an integration will also allow for a combination of direct and indirect phases within one optimization problem. This approach is especially attractive because a solution of such a problem does not require an explicit formulation of the transversality conditions and these are already included in the corresponding Karush–Kuhn–Tucker conditions of the SQP solver.

Acknowledgments

This research has been supported by the European Space Research and Technology Center (ESTEC). The Contract Monitor is Klaus Mehlem.

References

[1]Markl, A. W., "An Initial Guess Generator for Launch and Reentry Vehicle Trajectory Optimization," Ph.D. Dissertation, Inst. of Flight Mechanics and Control, Univ. of Stuttgart, Stuttgart, Germany, June 2001.

[2]McAdoo, S. F., Jr., Jezewski, D. J., and Dawkins, G. S., "Development of a Method for Optimal Maneuver Analysis of Complex Space Mission," NASA TN D-7882, April 1975.

[3]Brown, K. R., Harrold, E. F., and Johnson, G. W., "Rapid Optimization of Multiple-Burn Rocket Flights," IBM/NASA, NASA CR-1430, Sept. 1969.

[4]Calise, A. J., Melamed, N., and Lee, S., "Design and Evaluation of a Three-Dimensional Optimal Ascent Guidance Algorithm," *Journal of Guidance, Control, and Dynamics*, Vol. 21, No. 6, 1998, pp. 867–875.

[5]Gath, P. F., "Improvements to a Hybrid Algorithm for Rapid Generation of 3-D Optimal Launch Vehicle Ascent Trajectories," M.S. Thesis IFR_SR_98_016, Inst. of Flight Mechanics and Control, Univ. of Stuttgart, Stuttgart, Germany, Dec. 1998.

[6]Gath, P. F., and Calise, A. J., "Optimization of Launch Vehicle Ascent Trajectories with Path Constraints and Coast Arcs," *Journal of Guidance, Control, and Dynamics*, Vol. 24, No. 2, 2001, pp. 296–304.

[7]Gath, P. F., and Well, K. H., "HISTOS Technical Report 1," Inst. of Flight Mechanics and Control, Univ. of Stuttgart, TR 99-002, Stuttgart, Germany, June 1999.

[8]Gath, P. F., and Well, K. H., "Trajectory Optimization Using a Combination of Direct Multiple Shooting and Collocation," AIAA Paper 2001-4047, Aug. 2001.

[9]Bryson, A. E., Jr., and Ho, Y-C., *Applied Optimal Control*, Hemisphere, 1975, Chap. 2.

[10]"ASTOS Model Library Reference Manual," Inst. of Flight Mechanics and Control, Univ. of Stuttgart, ASTOS MLR 96-01.0, Stuttgart, Germany, July 1996.

[11]"ASTOS Conventional Launchers Application Manual," Inst. of Flight Mechanics and Control, Univ. of Stuttgart, ASTOS CLA 96-01.0, Stuttgart, Germany, July 1996.

[12]Well, K. H., Markl, A., and Mehlem, K., "ALTOS—A Trajectory Analysis and Optimization Software for Launch- and Reentry Vehicles," International Astronautical Federation, IAF-97-V4.04, Oct. 1997.

[13]Wiegand, A., Well, K. H., Mehlem, K., Steinkopf, M., and Ortega, G., "ALTOS—ESA's Trajectory Optimization Tool Applied to Reentry Vehicle Trajectory Design," International Astronautical Federation, IAF-99-A.6.09, Oct. 1999.

[14]"GESOP Software User Manual," Inst. of Flight Mechanics and Control, Univ. of Stuttgart, GESOP SUM 98-4.0, Stuttgart, Germany, Oct. 1998.

[15]Jänsch, C., Schnepper, K., and Well, K. H., "Multiphase Trajectory Optimization Methods with Applications to Hypersonic Vehicles," *Applied Mathematics in Aerospace Science and Engineering*, edited by A. Miele and A. Salvetti, Plenum, New York, 1994, Chap. 8.

C. A. Kluever
Associate Editor